ACS APPLIED MATERIALS & INTERFACES

Research Article

www.acsami.org

Hierarchical SnO_2 Nanoparticle-ZnO Nanorod Photoanode for Improving Transport and Life Time of Photoinjected Electrons in Dye-Sensitized Solar Cell

Nguyen Khac Huu, Dae-Yong Son, In-Hyuk Jang, Chang-Ryul Lee, and Nam-Gyu Park*

School of Chemical Engineering and Department of Energy Science, Sungkyunkwan University, Suwon 440-746, Korea

ABSTRACT: A hierarchical photoanode comprising a SnO_2 nanoparticle underlayer and a ZnO nanorod overlayer was prepared and its photovoltaic performance was compared to photoanodes consisting of SnO_2 nanoparticle only and ZnO nanorod only. The photoanode layer thickness was adjusted to about 7.6 μm to eliminate thickness effect. Ruthenium complex, coded N719, was used as a sensitizer. The photoanode composed of ZnO nanorod only showed a power conversion efficiency (PCE) as low as 0.54% with a short-circuit photocurrent density (J_{SC}) of 2.04 mA/cm^2 and an open-circuit voltage (V_{OC}) of 500 mV. The photoanode with SnO_2 nanoparticle only exhibited higher PCE (1.24%) because of higher J_{SC} (6.64 mA/cm^2), whereas V_{OC} (340 mV) was lower than ZnO nanorod. Compared to SnO_2 nanoparticle and ZnO nanorod films, the bilayer structured film demonstrated much higher PCE (2.62%) because of both higher J_{SC} (7.35 mA/cm^2) and V_{OC} (660 mV). Introduction of ZnO nanorod on the SnO_2 nanoparticle layer improved significantly electron transport and lifetime compared to the SnO_2 only film. One Order of magnitude slower charge recombination rate for the bilayer film than for the SnO_2 film was mainly responsible for the improved efficiency.

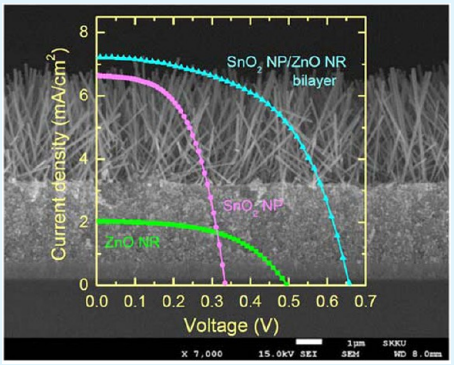

KEYWORDS: *dye-sensitized solar cell, ZnO, SnO_2, nanorod, bilayer, electron transport, recombination*

INTRODUCTION

Dye-sensitized solar cell (DSSC) developed by O'Regan and Grätzel in 1991[1] has received great attention during the last two decades because of eco-friendly and low-cost technology for solar energy conversion. A typical DSSC structure consists of a mesoporous TiO_2 photoanode whose surface is sensitized with dye, a redox electrolyte and a catalytic Pt-coated counter electrode. Semiconducting metal oxides other than TiO_2, including ZnO[2−12] and SnO_2,[13−17] have been also investigated as potential alternatives to TiO_2. However, the power conversion efficiencies (PCEs) based on ZnO were reported to be much lower than TiO_2 although the conduction band edge position of ZnO is similar to that of TiO_2. One of reasons for such a low performance is chemical instability of ZnO in acidic media. For the case of SnO_2, device performance was also low because of the inherent low conduction band edge, leading to theoretically low photovoltage, and the fast recombination process.[18] To overcome drawbacks in ZnO and SnO_2, core−shell and composite approaches were proposed. It was found that photovoltaic performance of SnO_2 was significantly improved by surface modification with insulating oxides.[19−22] A composite structure by adding ZnO nanoparticle to SnO_2 nanoparticle was found to improve photovoltage of SnO_2 because of upward shift of conduction band edge.[23] Although the composite film comprising ZnO and SnO_2 nanoparticles exhibited better performance compared to the isolated ZnO or SnO_2, it seems to be hard to control electron transport and charge recombination in such the randomly oriented nanoparticle admixed structure.

It was reported that a DSSC based on the ZnO nanorod structure with ruthenium N3 dye showed 1.5 times higher PCE than that for a similar device based on ZnO nanoparticles.[24] Intensity modulated photocurrent and photovoltage study confirmed that the better performance from ZnO nanorod was attributed to faster electron transport compared to colloidal ZnO nanoparticle.[25] A hierarchical layer structure comprising ZnO nanorod and SnO_2 nanoparticle is thus expected to regulate better electron transport and charge recombination compared to the random admixture film. Here, we report on preparation and photovoltaic performance of a hierarchical photoanode comprising bilayer structure of SnO_2 nanoparticle underlayer and ZnO nanorod overlayer. Electron transport and charge recombination of the bilayer structured photoanode are compared to those of photoanodes comprising SnO_2 nanoparticle only and ZnO nanorod only.

EXPERIMENTAL SECTION

Synthesis of ZnO Nanorods. ZnO rods were grown by two-step process. First, ZnO seed layer was formed on a fluorine-doped tin oxide (FTO) conductive glass (Pilkington, TEC-8, 8 Ω/sq) according to the methods described elsewhere.[2,26,27] A coating solution was

Received: November 16, 2012
Accepted: January 18, 2013
Published: January 18, 2013

   dx.doi.org/10.1021/am302729v | *ACS Appl. Mater. Interfaces* 2013, 5, 1038−1043

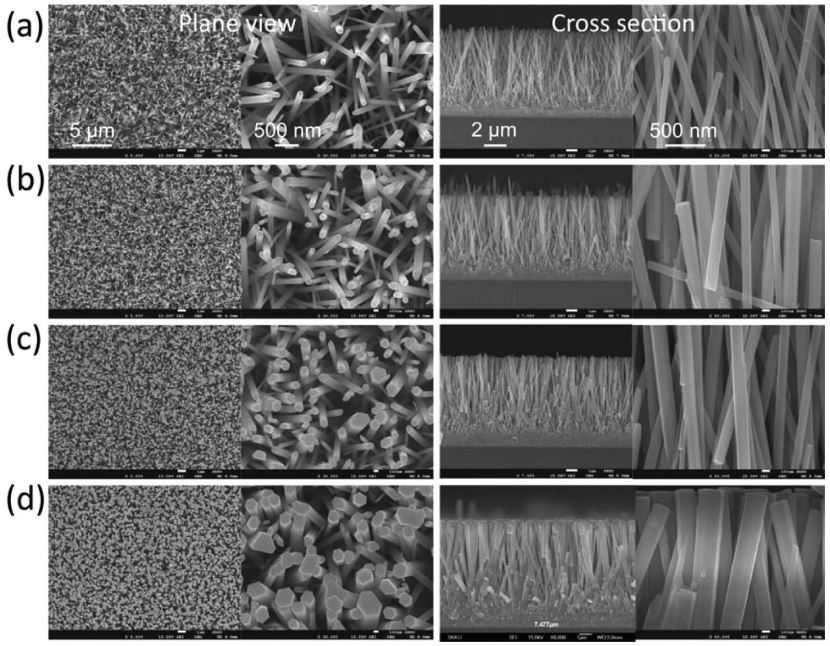

Figure 1. Plane and cross-sectional SEM images of ZnO nanorods depending on the precursor concentration of (a) 25, (b) 35, (c) 50, and (d) 100 mM of the zinc nitrate hydrate and HMTA admixed aqueous solution.

prepared by dissolving zinc acetate dihydrate ($Zn(CH_3COO)_2{\cdot}2H_2O$, Aldrich, 98%) in ethanol (5 mM), which was stirred for 2 h and then aged for 48 h at ambient temperature. The clear sol solution was spun on the FTO glass at 2500 rpm for 35 s, which was followed by curing on a hot plate at 150 °C for 10 min. The spin coating and curing process were repeated four times in order to obtain a dense and uniform film, which was finally annealed at 350 °C for 30 min. This layer was used as a seed layer for growing ZnO nanorod. The precursor solution for growing ZnO nanorod was prepared by dissolving zinc nitrate hexahydrate ($Zn(NO_3)_2{\cdot}6H_2O$, Aldrich, 98%) and hexamethylenetetramine (HMTA, Aldrich, 99%) in deionized water and stirring for 2 h. The equi-molar concentration of zinc nitrate and HMTA was varied from 25 mM to 100 mM. The FTO substrate with the ZnO seed layer was floated face-down in a bottle and aged for ca. 5 h at 80 °C in a constant temperature and humidity chamber. Upon completion of the reaction, the substrate was rinsed with deionized water and dried at 60 °C overnight and then heated at 350 °C for 30 min to get rid of the surfactant.

Synthesis of SnO_2 Nanoparticles. Nanocrystalline SnO_2 particles were hydrothermally synthesized as follows. A mixture of 100 mL of deionized water and 20.072 g of $SnCl_4{\cdot}5H_2O$ (Aldrich, 98%) was slowly added to the ammonium hydroxide solution that was prepared by mixing 77.9 mL of NH_4OH (Aldrich, ACS reagent, 28.0–30.0% NH_3 basis) with 120 mL of deionized water. The mixture was stirred for 2 h, where the solution pH reached 12 and the final concentration of $SnCl_4{\cdot}5H_2O$ and ammonium hydroxide was 0.2 and 2 M, respectively. The solution was transferred to a nonstirred titanium vessel and heated at 250 °C for 12 h using an autoclave (Parr Instrument). The white precipitate was washed with water until no detection of chloride ion using 0.1 M aqueous solution of $AgNO_3$. For preparing a screen-printable paste, water in the SnO_2 colloid solution was replaced by ethanol. Terpineol (Aldrich) and ethyl cellulose (Aldrich) were added to the ethanolic SnO_2 solution, followed by evaporation of ethanol using a rotary evaporator. The paste was further treated with three-roll-mill. The nominal composition of SnO_2/terpineol/ethyl cellulose was 1/4/0.5.

Preparation of SnO_2/ZnO Bilayer. The first layer (underlayer) was formed by deposition of the SnO_2 paste on the FTO glass and annealing at 550 °C for 1 h in air. On the top of the SnO_2 film, ZnO rod was grown by the same method described previously. The top of the SnO_2 layer was covered with the ZnO seed layer, which was treated with the 35 mM of zinc nitrate and HTMA mixed solution to grow ZnO nanorod. After that, the film was rinsed by deionized water and ethanol, and then annealed at 350 °C in 30 min for removing the surfactant.

Solar Cell Fabrication. The prepared electrodes were immersed in an ethanol solution containing 0.5 mM of N719 dye (cis-bis(isothiocyanato) bis (2,2′-bipyridyl-4,4′-dicarboxylic acid) ruthenium(II)) (Esolar, Taiwan) at 40 °C for 20 min. A counter electrode was prepared by spreading a droplet of 0.7 mM of $H_2PtCl_6{\cdot}6H_2O$ (Aldrich, 99.9%) in 2-propanol (Aldrich, 99.5%), which was heated at 400 °C for 20 min. The dye-coated electrode and the Pt counter electrode were sealed with 60 μm Surlyn (solaronix, meltonix 1170–60) at pressure of 2.3 bar and temperature of about 90 °C. The used electrolyte was composed of 0.7 M 1-methyl-3-propylimidazolium iodide (MPII), 0.03 M I_2 (Aldrich, 99.9%), 0.05 M guanidinium thiocyanate (GSCN) (Aldrich, 97%) and 0.5 M 4-t-butylpyridine (Aldrich, 98%) in acetonitrile (Aldrich, 99.8%) and valeronitrile (Aldrich, 99.5%) (85: 15 volume ratio).

Characterization. The amount of the adsorbed dye was estimated by a UV–vis spectrophotometer (Agilent 8453), where the adsorbed dye was desorbed using 0.05 M NaOH in toluene and ethanol (v/v 1:1). The surface and cross-sectional images of the photoanodes were investigated using a field-emission scanning electron microscope under accelerating voltage of 15 kV (FE-SEM, JEOL, JSM-7600F). Photocurrent and voltage were measured from a solar simulator equipped with 450 W xenon lamp (Newport 6279NS) and a Keithley 2400 source meter. Light intensity was adjusted with a NREL-calibrated Si solar cell having KG-2 filter for approximating AM 1.5G one sun light intensity (100 mW/cm^2). While measuring current and voltage, the cell was covered with a black mask having an aperture. Incident photon-to-electron conversion efficiency (IPCE) was measured by using an IPCE system (PV measurement Inc.) under DC mode, where a 75 W xenon lamp was used as a light source for generating monochromatic beam. Time constants for electron transport and recombination were obtained using a photocurrent and photovoltage transient spectroscopy.[28] The cells were probed with a weak laser pulse at 532 nm superimposed on a relatively large, back ground (bias) illumination at 680 nm. The bias light was illuminated by a 0.5 W diode laser (B&W TEK Inc., model BWF1-670-300E/55370). The intensity of the bias light was adjusted using ND filters (neutral density filters). The 680 nm bias light is only weakly absorbed by the dye, and therefore the injected electrons are introduced into a narrow spatial region of the film, corresponding to where the probe

light enters the film. A 30 mW frequency-doubled Nd:YAG laser (Laser-Export Co. Ltd. Model: LCS-DTL-314QT) (λ = 532 nm, pulse duration 10 ns) was used as probe light. The photocurrent transients were obtained by using a Stanford Research Systems model SR570 low-noise current preamplifier, amplified by a Stanford Research Systems model SR560 low-noise preamplifier, and recorded on Tektronics TDS 3054B digital phosphore oscilloscope 500 MHz 5GS/s DPO. The photovoltage transients were obtained by using SR560 preamplifier, which was recorded on oscilloscope combined with Keithley 2400 measure unit. The photocurrent- and the photovoltage−time curves were fitted with an exponential relationship, $y(t) = \exp(-t/\tau)$, where y represents photocurrent density or photovoltage, t is time and τ (τ_C for electron transport and τ_R for recombination) is constant.

RESULTS AND DISCUSSION

Figure 1 shows plane and cross-sectional view of the ZnO nanorods grown on the FTO substrate. It is clearly seen that ZnO nanorod is vertically grown on the FTO substrate. The diameter of hexagon-like ZnO nanorod is increased with increasing zinc nitrate and HTMA concentration. However, almost no change in length is observed. On the other hand, the diameter of ZnO nanorod is significantly altered by the precursor and surfactant concentration. The results indicate that the change in precursor solution concentration at the given temperature of 80 °C and duration of 6 h affects mostly diameter of the ZnO nanorod without change in length of the ZnO nanorod. ZnO nanorod grows with hexagonal morphology that is evident as the precursor concentration increases. It was reported that both the surface property of seed layer and the solution environment were crucial to the evolution of ZnO morphologies,[29,30] where hexagonal morphology was found to be preferred by solution growth using zinc nitrate hydrate.[26,31]

Dependence of diameter and length of ZnO nanorod on the precursor concentration is plotted in Figure 2. Diameter is

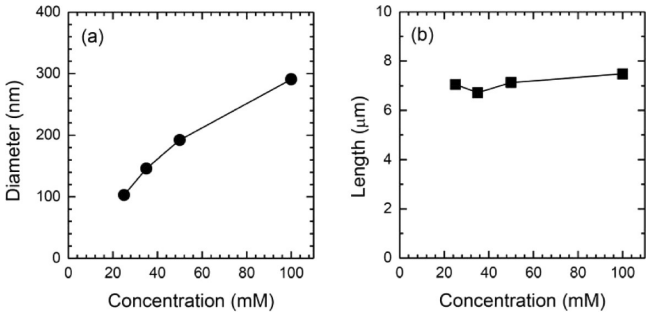

Figure 2. Effect of the precursor concentration on diameter and length of ZnO nanorod. The growth of nanorod was carried out at constant temperature of 80 °C and duration of 6 h.

linearly increased with concentration, while length is invariant with concentration. Diameter of the ZnO nanorod increases from 103 to 146 nm, 192 and 291 nm as the precursor concentration increases from 25 mM to 35 mM, 50 mM and 100 mM, respectively. Length of the ZnO rod is about 7 μm regardless of the precursor concentration. It is obvious that change in concentration affects mainly the diameter of ZnO nanorod.

Effect of diameter of ZnO nanorod on photovoltaic performance is compared in Figure 3 and photovoltaic parameters are listed in Table 1. Photocurrent density (J_{SC}) increases with increasing the diameter from 103 nm (grown from 25 mM) to 146 nm (grown from 35 mM). Further

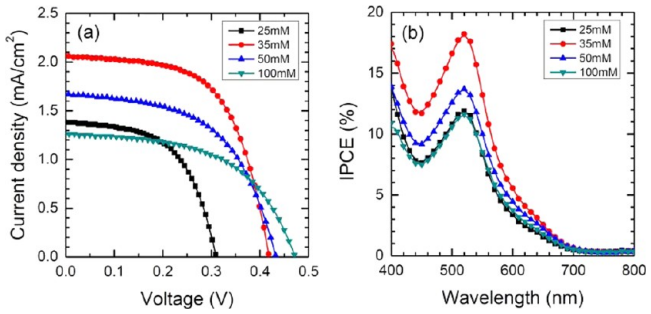

Figure 3. Current−voltage curves and IPCE spectra of the ZnO rod based DSSCs, depending on the precursor concentration.

Table 1. Photovoltaic Parameters of the ZnO Nanorod-Based DSSCs, Depending on the Precursor Concentration

precursor concentration (diameter)	J_{SC} (mA/cm^2)	V_{OC} (V)	fill factor	PCE (%)	area (cm^2)	thickness (μm)
25 mM (103 nm)	1.39	0.31	0.56	0.24	0.358	7.1
35 mM (146 nm)	2.06	0.42	0.60	0.52	0.302	6.7
50 mM (192 nm)	1.69	0.43	0.54	0.39	0.347	7.1
100 mM (291 nm)	1.26	0.47	0.54	0.32	0.334	7.5

increase in the diameter leads to low J_{SC}. Open-circuit voltage (V_{OC}) increases with increasing the diameter. The increased J_{SC} correlates with the increased amount of the adsorbed dye as can be seen in Figure 4. Low dye loading on the smallest diameter

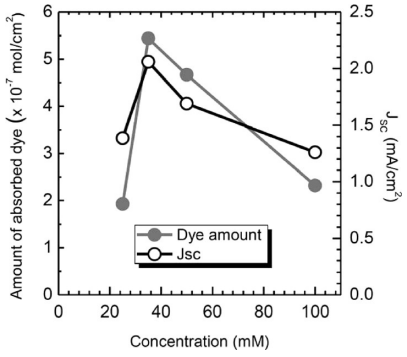

Figure 4. Amount of adsorbed dye on ZnO nanorods and J_{SC} as a function of the precursor concentration.

is probably due to low density of rod, as can be seen in the plane view of SEM in Figure 1a, leading to low total surface area in spite of small diameter. The decrease in dye loading with increasing diameter to 192 nm (from 50 mM) and 291 nm (from 100 mM) is ascribed to the decreased surface area. Significant increase in V_{OC} from 103 to 146 nm is due to in part the increased diameter, associated with the decreased surface state, and the higher photocurrent density. A slight increase in V_{OC} upon further increase in diameter can be explained by the reduced surface state due to the increased diameter. The fill factor is slightly declined as the precursor concentration increases, which is associated with a decreased porosity as can be seen in Figure 1. ZnO nanorod with diameter of 146 nm (from 35 mM) exhibits highest efficiency. However, the PCE is

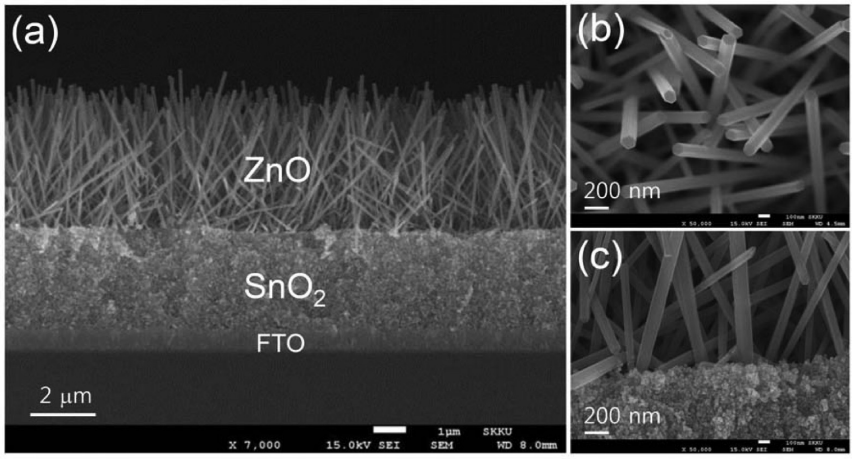

Figure 5. (a) Cross-sectional SEM image of the bilayer comprising the SnO_2 nanoparticle underlayer and the ZnO nanorod overlayer, (b) plane view of the ZnO nanorod layer, and (c) interface between SnO_2 nanoparticle and ZnO nanorod.

as low as the reported ZnO-based DSSCs whose efficiencies were less than 1% without modification of ZnO surface.

Because the photovoltaic performance of photoanode comprising ZnO nanorod only is poor, a bilayer structure has been considered to improve the performance. For bilayer construction, an efficient electron transport across the entire oxide electrode layer should be taken into consideration. SnO_2 is selected for this purpose because of lower conduction band edge energy than ZnO. SnO_2 nanoparticulate layer (ca. 3 μm) is first deposited on FTO substrate and ZnO nanorod is grown on the top of the SnO_2 layer. Figure 5 shows SEM images of the bilayer structure, where ZnO nanorod is almost vertically grown on the SnO_2 layer. We select 35 mM precursor solution to grow ZnO nanorod because 35 mM solution showed best performance in the previous study. The length of ZnO nanorod is ca. 4.4 μm. Total thickness of the bilayer is controlled to be about 7.4 μm in order to compare the performance of the ZnO nanorod only (7−7.5 μm). ZnO nanorods are well in contact with SnO_2 nanoparticles as can be seen in the SEM image in Figure 5c.

Prior to investigation of photovoltaic performance of the bilayer electrode, photoanode comprising only SnO_2 layer is prepared and its photovoltaic performance is investigated. Figure 6 shows the effect of SnO_2 film thickness on J_{SC} and efficiency. Both J_{SC} and efficiency increase as the SnO_2 film thickness increases up to 8 μm, whereas a decline in performance is observed for the films thicker than 8 μm.

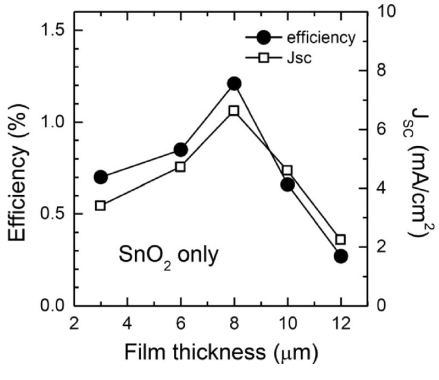

Figure 6. Power conversion efficiency and J_{SC} as a function of the SnO_2 film thickness.

This is well consistent with the previous result.[21] The main drawback for the SnO_2 based DSSC is low *Voc* due to lower conduction band edge than TiO_2 (about 0.4 eV lower than TiO_2). To solve the problem of low V_{oc}, surface modification of SnO_2 (core−shell structure) has been proposed;[20−22] however, shell thickness is critical in the photovoltaic performance and hard to control.

Photovoltaic performance of the SnO_2 nanoparticle (NP)/ZnO nanorod (NR) bilayer is compared with that of the ZnO NR only and the SnO_2 NP only. The bilayer structure shows J_{SC} of 7.35 mA/cm^2, V_{oc} of 0.66 V and fill factor of 0.54, resulting in a conversion efficiency of 2.62%, which is higher than the efficiency of ZnO only (0.54%) and SnO_2 only (1.24%). Absolute IPCE is higher in the measured entire wavelength for the bilayer structure than the ZnO nanorod and SnO_2 nanoparticle films (Figure 7b). It is noted that V_{OC} of the

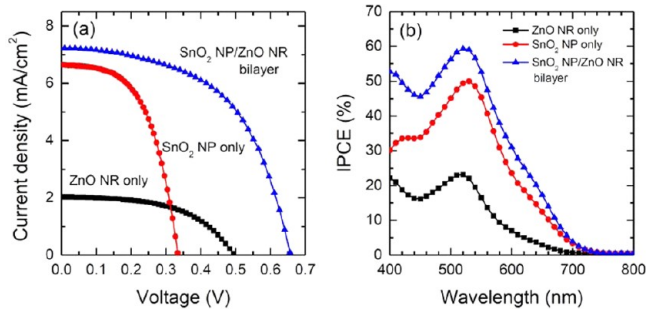

Figure 7. (a) Current−voltage curves and (b) IPCE spectra for the DSSCs based on the ZnO nanorod (NR), the SnO_2 nanoparticle (NP), and the SnO_2 NP/ZnO NR bilayer.

bilayer structure is two times higher than SnO_2 only (0.34 V) and also 160 mV higher than ZnO only (0.5 V). It was reported that V_{oc} was enhanced by deposition of thin layer of ZnO on nanocrystalline SnO_2 surface[22] or by addition of ZnO particle to SnO_2 nanoparticle.[23] The former was explained by suppression of charge recombination, while the latter was explained by negative shift of conduction band edge of SnO_2. The *Voc* enhancement from the SnO_2/ZnO bilayer structure may be related to either enhanced electron lifetime, associated with suppression of charge recombination, or negative shift of SnO_2 conduction band by addition of ZnO nanorod. Because

the present bilayer structure is different from the mixed SnO_2 and ZnO particles,[23] we assume that the V_{oc} enhancement may be related to charge recombination. Electron lifetime is thus measured to elucidate the origin of the V_{oc} enhancement in SnO_2/ZnO bilayer structure.

Table 2. Photovoltaic Parameters for the DSSCs Based on the ZnO Nanorod (NR), the SnO_2 Nanoparticle (NP), and the SnO_2 NP/ZnO NR Bilayer

electrode	Jsc (mA/cm^2)	Voc (V)	fill factor (%)	PCE (%)	area (cm^2)	thickness (μm)
ZnO	2.04	0.50	0.53	0.54	0.349	7.8
SnO_2	6.64	0.34	0.55	1.24	0.362	7.6
SnO_2 /ZnO	7.35	0.66	0.54	2.62	0.327	7.4

To investigate electron transport and charge recombination in the bilayer structure, we measured electron diffusion coefficient and charge recombination time constant. As shown in Figure 8, electron diffusion coefficient is highest in

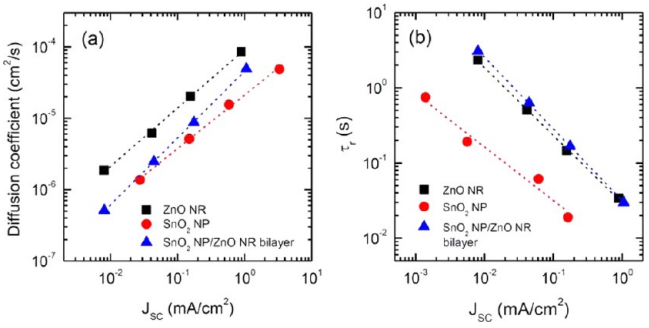

Figure 8. (a) Electron diffusion coefficients and (b) time constants for charge recombination (τ_r) for the DSSCs based on the ZnO nanorod (NR), the SnO_2 nanoparticle (NP), and the SnO_2 NP/ZnO NR bilayer.

ZnO nanorod and lowest in SnO_2 nanoparticle, which underlines that nanorod structure is beneficial for fast electron transport. Electrons in the bilayer structure are not faster than ZnO nanorod but slightly faster than SnO_2 film. On the other hand, electron lifetime is significantly improved in the bilayer structure as can be seen in Figure 8b, which is 1 order of magnitude higher than that in the SnO_2 film. Suppression of charge recombination for the bilayer structure is even better than ZnO nanorod. Compared to the SnO_2 only film, the much longer electron lifetime in the SnO_2/ZnO bilayer structure is due to mainly the presence of ZnO nanorod and in part surface modification of the SnO_2 underlayer during growth of ZnO nanorod in zinc nitrate solution. This significant improvement for electron lifetime is responsible for the high V_{OC} for the bilayer structure. Long electron lifetime is expected to contribute to long electron diffusion length, which will lead to the improved charge collection efficiency, associated with high J_{SC}.

CONCLUSION

We fabricated a bilayer structure consisted of the SnO_2 nanoparticle underlayer and the ZnO nanorod overlayer and its photovoltaic performance was compared to the single layered photoanode such as SnO_2 nanoparticle only or ZnO nanorod only. Compared to SnO_2 nanoparticle and ZnO nanorod films, the bilayer structured film exhibited higher J_{SC} and V_{OC}, leading to higher PCE. Slow electron transport and fast recombination were drawback in SnO_2 nanoparticle film, which was overcome by introduction of ZnO nanorod on the top of SnO_2 nanoparticle layer. Electron diffusion coefficient became faster and charge recombination rate was 1 order of magnitude slower for the bilayer structure than that of the SnO_2 nanoparitcle film. From this study, modification of nanostructured layer in dye-sensitized solar cell was found to have a significant effect on electron transport and charge recombination.

AUTHOR INFORMATION

Corresponding Author

*E-mail: npark@skku.edu. Tel: +82-31-290-7241. Fax: +82-31-290-7272.

Author Contributions

N.K.H., D.-Y.S., and I.-H.J. contributed equally to this work. C.-R.L. measured transient photocurrent and voltage spectroscopy.

Notes

The authors declare no competing financial interest.

ACKNOWLEDGMENTS

This work was supported by the National Research Foundation of Korea (NRF) grant funded by the Ministry of Education, Science and Technology (MEST) of Korea under Contracts 2012-0005601, R31-2008-10029 (WCU program), and the Global Frontier R&D Program on Center for Multiscale Energy System.

REFERENCES

(1) O'Regan, B.; Grätzel, M. *Nature* **1991**, *353*, 737−740.
(2) Law, M.; Greene, L. E.; Johnson, J. C.; Saykally, R.; Yang, P. *Nat. Mater.* **2005**, *4*, 455−459.
(3) Rensmo, H.; Keis, K.; Lindstrom, H.; Sodergren, S.; Solbrand, A.; Hagfeldt, A.; Lindquist, S.-E.; Wang, L. N.; Muhammed, M. *J. Phys. Chem. B* **1997**, *101*, 2598−2601.
(4) Keis, K.; Magnusson, E.; Lindstrom, H.; Lindquist, S.-E.; Hagfeldt, A. *Sol. Energ. Mat. Sol. C.* **2002**, *73*, 51−58.
(5) Martinson, A. B. F.; Elam, J. W.; Hupp, J. T.; Pellin, M. J. *Nano Lett.* **2007**, *7*, 2183−2187.
(6) Zhang, Q. F.; Dandeneau, C. S.; Zhou, X. Y.; Cao, G. Z. *Adv. Mater.* **2009**, *21*, 4087−4108.
(7) Hosono, E.; Fujihara, S.; Honna, I.; Zhou, H. S. *Adv. Mater.* **2005**, *17*, 2091−2094.
(8) Quintana, M.; Edvinsson, T.; Hagfeldt, A.; Boschloo, G. *J. Phys. Chem. C* **2007**, *111*, 1035−1041.
(9) Baxter, J. B.; Aydil, E. S. *Sol. Energy Mater. Sol. Cells* **2006**, *90*, 607−622.
(10) Jiang, C. Y.; Sun, X. W.; Lo, G. Q.; Kwong, D. L.; Wang, J. X. *Appl. Phys. Lett.* **2007**, *90*, 263501.
(11) Yoshida, T.; Minoura, H. *Adv. Mater.* **2000**, *12*, 1219−1222.
(12) Kakiuchi, K.; Hosono, E.; Fujihara, S. *J. Photochem. Photobiol. A* **2006**, *179*, 81−86.
(13) Chappel, S.; Zaban, A. *Sol. Energy Mater. Sol. Cells* **2002**, *71*, 141−152.
(14) Chappel, S.; Chen, S.-G.; Zaban, A. *Langmuir* **2002**, *18*, 3336−3342.
(15) Shang, G.; Wu, J.; Huang, M.; Lin, J.; Lan, Z.; Huang, Y.; Fan, L. *J. Phys. Chem. C* **2012**, *116*, 20140−20145.
(16) Wijeratne, K.; Akilavasan, J.; Thelakkat, M.; Bandara, J. *Electrochim. Acta* **2012**, *72*, 192−198.
(17) Fukai, Y.; Kondo, Y.; Mori, S.; Suzuki, E. *Electrochem. Commun.* **2007**, *9*, 1439−1443.

(18) Green, A. N. M.; Palomares, E.; Haque, S. A.; Kroon, J. M.; Durrant, J. R. *J. Phys. Chem. B* **2005**, *109*, 12525−12533.
(19) Prasittichai, C.; Hupp, J. T. *J. Phys. Chem. Lett.* **2010**, *1*, 1611−1615.
(20) Kay, A.; Grätzel, M. *Chem. Mater.* **2002**, *14*, 2930−2935.
(21) Park, N.-G.; Kang, M. G.; Ryu, K. S.; Kim, K. M.; Chang, S. H. *J. Photoch. Photobio. A* **2004**, *161*, 105−110.
(22) Park, N. G.; Kang, M. G.; Kim, K. M.; Ryu, K. S.; Chang, S. H.; Kim, D. K.; van de Lagemaat, J.; Benkstein, K. D.; Frank, A. J. *Langmuir* **2004**, *20*, 4246−4253.
(23) Niinobe, D.; Makari, Y.; Kitamura, T.; Wada, Y.; Yanagida, S. *J. Phys. Chem. B* **2005**, *109*, 17892−17900.
(24) Seow, Z. L. S.; Wong, A. S. W.; Thavasi, V.; Jose, R.; Ramakrishna, S.; Ho, G. W. *Nanotechnology* **2009**, *20*, 045604.
(25) Martinson, A. B. F.; McGarrah, J. E.; Parpia, M. O. K.; Hupp, J. T. *Phys. Chem. Chem. Phys.* **2006**, *8*, 4655−4659.
(26) Greene, L. E.; Law, M.; Goldberger, J.; Kim, F.; Johnson, J. C.; Zhang, Y.; Saykally, R. J.; Yang, P. *Angew. Chem., Int. Ed.* **2003**, *42*, 3031−3034.
(27) Greene, L. E.; Law, M.; Tan, D. H.; Montano, M.; Goldberger, J.; Somorjai, G.; Yang, P. *Nano Lett.* **2005**, *5*, 1231−1236.
(28) Kim, M.-J.; Lee, C.-R.; Jeong, W.-S.; Im, J.-H.; Ryu, T. I.; Park, N.-G. *J. Phys. Chem. C* **2010**, *114*, 19849−19852.
(29) Gao, Y.; Nagai, M. *Langmuir* **2006**, *22*, 3936−3940.
(30) Plakhova, T. V.; Shestakov, M. V.; Baranov, A. N. *Inorg. Mater.* **2012**, *48*, 469−475.
(31) Chander, R.; Raychaudhuri, A. K. *J. Mater. Sci.* **2006**, *41*, 3623−3630.